

Supporting information for

**Joule heating driven infrared switching in flexible VO<sub>2</sub> nanoparticle  
film with reduced energy consumption for smart windows**

*Nan Shen,<sup>1,2</sup> Shi Chen,<sup>1</sup> Weijun Wang,<sup>1</sup> Run Shi,<sup>1</sup> Pengcheng Chen,<sup>1</sup> Dejun Kong,<sup>1</sup>*

*Yuxing Liang,<sup>1</sup> Abbas Amini,<sup>3</sup> Jianbo Wang,<sup>2</sup> Chun Cheng<sup>1\*</sup>*

1. Department of Materials Science and Engineering, Southern University of Science and Technology, Shenzhen 518055, P. R. China
2. School of Physics and Technology, Wuhan University, Wuhan 430072, P. R. China
3. Center for Infrastructure Engineering, Western Sydney University, Kingswood, New South Wales, 2751, Australia.

\* Corresponding author. Chun Cheng, Southern University of Science and Technology, *E-mail*: chengc@sustc.edu.cn, Tel: +86-755-8801-8568.

**Contents:**

- 1. Schematic diagram of two-terminal VO<sub>2</sub>/ITO structure for applying voltage (Figure S1).**
- 2. Film with 2.0 wt.% VO<sub>2</sub> nanoparticles at 25 °C and 90 °C, along with their transmittance spectra (Figure S2).**
- 3. Thermochromic performance of VO<sub>2</sub> nanoparticle films (Table S1).**
- 4. The schematic diagram of infrared transmission of VO<sub>2</sub> films at ambient temperature of 52 °C (Figure S3).**
- 5. The stability of transmittance-temperature loops at 1200nm (T<sub>1200</sub>) of VO<sub>2</sub> nanoparticle films (Figure S4).**
- 6. The calculation method of curvature radius and the induced strain (Figure S5).**
- 7. The evaluated radius of curvature, strain and strain rate of flexible VO<sub>2</sub> film (Table S2).**

## 1. Schematic diagram of two-terminal VO<sub>2</sub>/ITO structure for applying voltage.

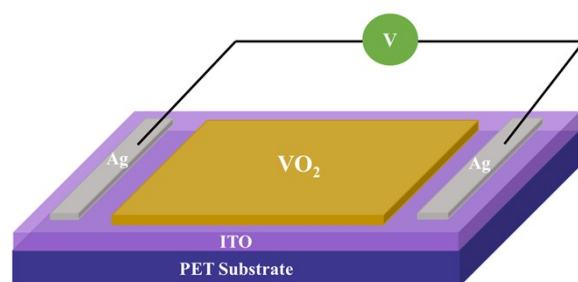


**Figure S1** Schematic diagram of two terminal VO<sub>2</sub>/ITO structure.

**Figure S1** shows the schematic diagram of a two terminal VO<sub>2</sub>-ITO structure, where copper wires were electrically connected to marginal ITO via silver paste, by which joule heating was effectively regulated by the applied voltage.

## 2. Film with 2.0 wt.% VO<sub>2</sub> nanoparticles at 25 °C and 90 °C, along with their transmittance spectra.

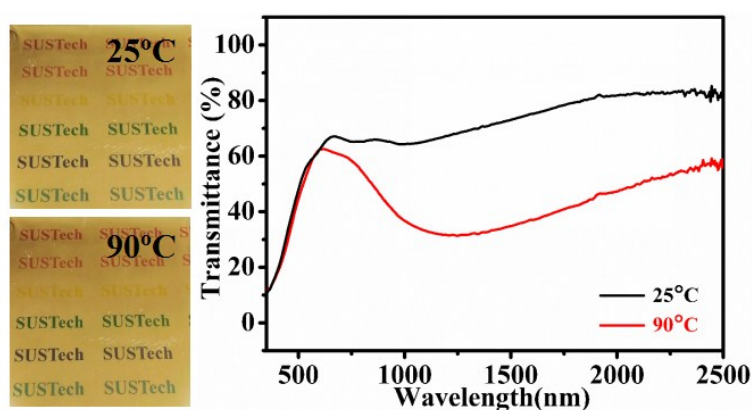


**Figure S2** Film with 2.0 wt.% VO<sub>2</sub> nanoparticles at 25 °C and 90 °C, along with their transmittance spectra.

**Figure S2** shows the photos of VO<sub>2</sub> films with almost unchanged visible transparency across the MIT.

## 3. Thermochromic performance of VO<sub>2</sub> nanoparticle films.

**Table S1** The integral luminous transmittance ( $T_{lum}$ ), solar energy modulation ability ( $\Delta T_{sol}$ ), and film thickness of VO<sub>2</sub> nanoparticle films with different solid contents.

Solid content of VO <sub>2</sub> (wt. %)	T <sub>lum</sub> (%)		T <sub>sol</sub> (%)		ΔT <sub>sol</sub> (%)	Film thickness (nm)
	25 °C	90 °C	25 °C	90 °C		
0.5	87.3	87.6	87.4	81.9	5.5	972
1.0	74.0	74.7	75.1	66.8	8.3	1042
2.0	57.3	55.5	60.2	46.4	13.8	1132
3.0	44.2	42.3	48.2	33.4	14.8	1238
3.5	36.2	34.4	41.0	26.5	14.5	1327

**4. The schematic diagram of infrared transmission of VO<sub>2</sub> films at ambient temperature of 52 °C.**

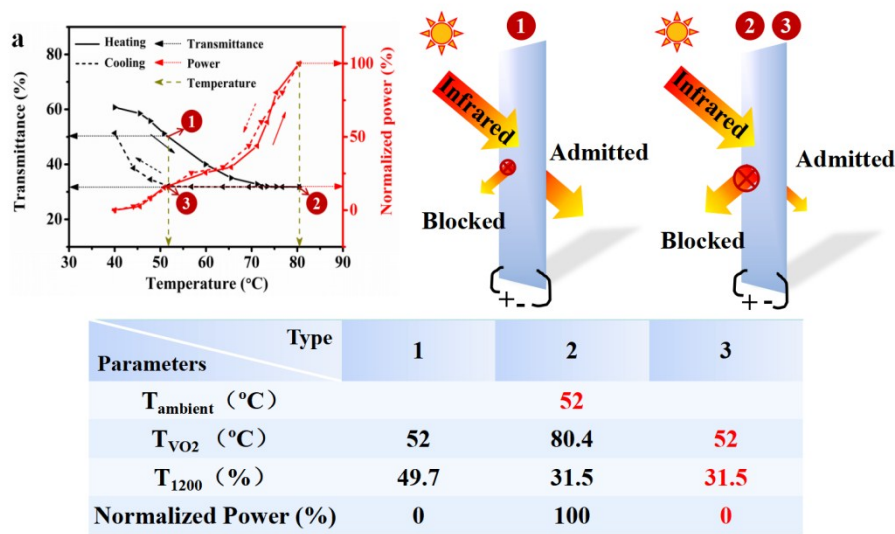


**Figure S3** Schematic diagram of infrared transmission of VO<sub>2</sub> films at ambient temperature of 52 °C (Sites ①, ②, ③).

**5. The stability of hysteresis loops of transmittance at 1200nm (T<sub>1200</sub>) of VO<sub>2</sub> nanoparticle films.**

The stability of the transmittance-temperature hysteresis loop at 1200nm of VO<sub>2</sub> film was explored in **Figure S4**. After 100 cycles, both the routine hysteresis loop (20

°C - 80 °C - 20 °C, red and blue curves) and the working loop in practical application (80 °C - 40 °C - 80 °C, dark yellow curves) were observed to be comparably stable, without obvious variations.

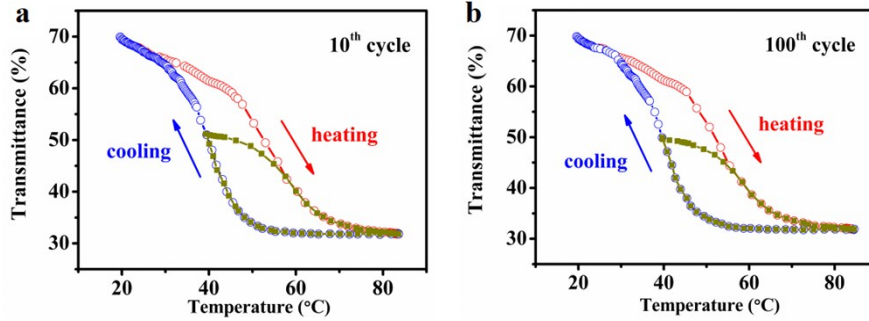


**Figure S4** The  $T_{1200}$ -temperature hysteresis loops in 10<sup>th</sup> (a) and 100<sup>th</sup> (b) cycle. Red and blue curves stand for  $T_{1200}$  in the heating (20 °C to 80 °C) and cooling (80 °C to 20 °C) processes, respectively. Dark yellow curves in each cycle denotes  $T_{1200}$  in an unconventional cycle, where the temperature initially declines from 80 °C to 40 °C and then returns back to 80 °C.

## 6. The calculation method of curvature radius and the induced strain.

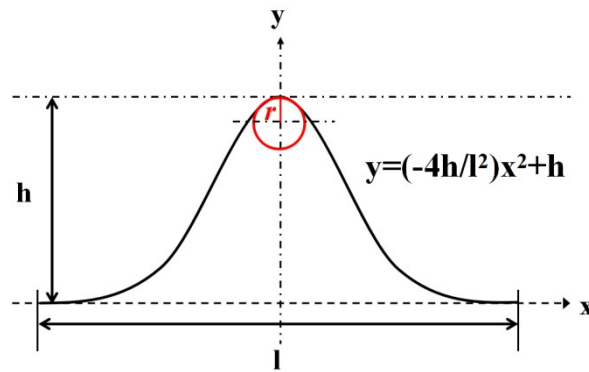


**Figure S5** The parabolic model used for estimating the radius of curvature at the vertex of parabolic curve.

The radius of curvature was calculated from the equation below

$$r = \left| \frac{(1+y'^2)^{3/2}}{y''} \right|$$

where  $y'$  and  $y''$  are first-order and second-order differential derivations of the parabolic function.

The strain (%) was calculated from the equation below<sup>1</sup>

$$\text{Strain}(\%) = \frac{\text{Total thickness of film}}{2 \times \text{radius of curvature}} \times 100$$

According to the above equations, the radius of curvature and strain were calculated, as shown in **Table S2**. The minimum  $r$  and maximum strain are found when the length of VO<sub>2</sub> film under bending test decreased to 16mm. This was chosen to conduct different bending cycles for the mechanical flexibility in this study.

## 7. The evaluated radius of curvature, strain and strain rate of flexible VO<sub>2</sub> film

**Table S2** The estimated radius of curvature ( $r$ ) according to  $h$  and  $l$ , the strain and strain rate of flexible VO<sub>2</sub> film upon bending.

$l$ (mm)	$h$ (mm)	$r$ (mm)	Strain (%)	Strain rate (%/s)
35	0	$\infty$	0	0
30	7.0	16	0.6	0.12
25	11	7.1	1.2	0.12
22	12	5.0	1.8	0.2
19	13	3.5	2.5	0.23
16	14	2.3	3.8	0.43

## Reference

1. Y. Ji, Y. Yang, S. K. Lee, G. Ruan, T. W. Kim, H. Fei, S. H. Lee, D. Y. Kim, J. Yoon and J. M. Tour, *ACS Nano*, 2016, **10**, 7598-7603.